

Unsupervised detection of non-iris occlusions[☆]



Michal Haindl^{a,*}, Mikuláš Krupička^{a,b}

^a The Institute of Information Theory and Automation of the Czech Academy of Sciences, 182 08 Prague, Czech Republic

^b Faculty of Information Technology, Czech Technical University, 160 00 Prague, Czech Republic

ARTICLE INFO

Article history:

Received 9 June 2014

Available online 5 March 2015

Keywords:

Iris recognition

Color

Markov random field

Texture

ABSTRACT

This paper presents a fast precise unsupervised iris defects detection method based on the underlying multispectral spatial probabilistic iris textural model and adaptive thresholding applied to demanding high resolution mobile device measurements. The accurate detection of iris eyelids and reflections is the prerequisite for the accurate iris recognition, both in near-infrared or visible spectrum measurements. The model adaptively learns its parameters on the iris texture part and subsequently checks for iris reflections using the recursive prediction analysis. The method is developed for color eye images from unconstrained mobile devices but it was also successfully tested on the UBIRIS v2 eye database. Our method ranked first from the 97+1 recent Noisy Iris Challenge Evaluation contest alternative methods on this large color iris database using the exact contest data and methodology.

© 2015 Elsevier B.V. All rights reserved.

1. Introduction

Biometrics based human identification systems have ever growing importance in recent trends toward more secure modern information society. Diverse biometric data can be exploited for numerous practical applications, such as bank access, airport entry points, or criminal evidence gathering but also for smart homes, cars control, or handicapped help systems. It can be human voice, fingerprint, eye, face, gait, veins, handwriting and many more. Various biometric data differ in ways how to acquire them, their durability, reliability, safety, and necessary technology for their acquisition and evaluation. In this work we focus on preprocessing part of the iris recognition—iris defect detection. The possibility for the eye-based human identification was originally suggested by Alphonse Bertillon [30] and subsequently pointed out by several others [1], the first method was published and patented by Daugman [8], and later estimated that the probability of two similar iris is 1 in 10^{72} [24]. For recent surveys of the iris recognition results see [3,4,30]. The overview of open iris databases can be found in [30].

The iris identification is complex task containing several sub-tasks (see the processing schema on Fig. 1 with iris defect detection elaborated part) that have to be solved. The whole process starts with image acquisition which hardly produces ideal noise-free, focused, and homogeneously illuminated images, thus the corresponding preprocessing steps for data normalization, denoising, or geometric

corrections are inevitable before the iris segmentation can be performed. Iris acquisition cameras use either near infrared (NR, 700–900 [nm]) or visible wavelength (VW, 390–700 [nm]) sensors each having some advantages and drawbacks. NR can penetrate iris surface and reveals well dark-colored irides, VW sensors on the other hand are ubiquitous, less hazardous to eye damage [23], and can be used for long distance observations. The reflectance properties of both spectra ranges differ which leads to different iris recognition pipelines. The rough iris segmentation results are typically coordinates of two circles, inner and outer border of iris. Additionally, a normalization step has been introduced to simplify the subsequent processing steps. Normalization is usually done transforming the iris into a fixed size rectangle. The selected features are then computed from the normalized rectangle and used in a classifier to recognize a corresponding human.

Unconstrained iris measurements contain numerous occlusion defects such as eyelid, eyelash, and reflections which have to be detected in the preprocessing step of any iris recognition algorithm. Undetected occlusions would otherwise confuse the recognition method and impair its recognition rate. While the unconstrained visible wavelength iris image acquisition is cheap and widely available it requires more demanding iris processing methods to achieve comparable recognition rate with optimal acquisition conditions in the controlled environment.

1.1. Iris defects detection

Unconstrained iris measurements inevitably introduce various sensing imperfections, such as reflections, upper/lower eyelids or

[☆] This paper has been recommended for acceptance by Gabriella Sanniti di Baja.

* Corresponding author. Tel: +420 2 6605 2350; fax: +420 2 8468 3031.

E-mail addresses: haindl@utia.cz (M. Haindl), krupimik@utia.cas.cz (M. Krupička).

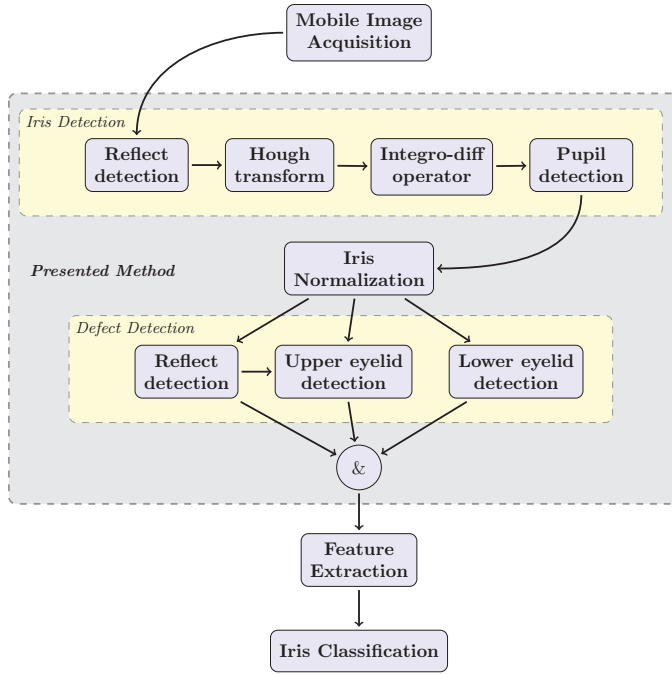


Fig. 1. Iris recognition processing pipeline.

eyelashes occlusions, or eyelid shadows. Such undetected defects significantly degrade iris classifiers performance. Thus it is necessary to remove such areas from the iris texture prior to the classification process what constitutes one of the most challenging problems in the iris recognition research [24]. Some detection methods are specialized to single imperfection category only, while others [5,9,13,16,18–20,26,31,34,35] can detect several types of imperfections.

Methods focused only on reflections are based on (adaptive) thresholding (e.g. [32]). Eyelid detectors are mostly based on edge detection followed with polynomial fitting (e.g. [10,37]). Chen et al. [6] or He et al. [15] proposed methods of eyelash detection based on simple thresholding. One of the first general imperfection detection methods was presented by Proenca and Alexandre [26]. His method is based on training classifier on manually detected irises and the eye representation is based on textural GLCM [14] features and the detector uses a neural network classifier.

The conventional approach for defect detection [7] is to compute a texture features in a local sub-window and to compare them with the reference values representing a perfect pattern. The method [22] preprocesses a gray level texture with histogram modification and median filtering. The image is subsequently thresholded using the adaptive filter and finally smoothed with another median filter run. Another approach for detection of gray level textured defects using linear FIR filters with optimized energy separation was proposed in [17]. Similarly the defect detection [33] is based on a set of optimized filters applied to wavelet sub-bands and tuned for a defect type. Method [11] uses translation invariant 2D RI-Spline wavelets for textile surface inspection. The gray level texture is removed using the wavelet shrinkage approach and defects are subsequently detected by simple thresholding. Contrary to above approaches the presented method uses the visible wavelength multispectral information.

Recent state-of-the-art non-iris occlusions detectors were mostly competing in the 2008 NICE.I (Noisy Iris Challenge Evaluation) focusing especially on detection accuracy. Nearly hundred various methods from 22 countries were submitted to this challenge and the best-ranked algorithms were published in [28]. The presented method uses results of these best-ranked algorithms for comparison.

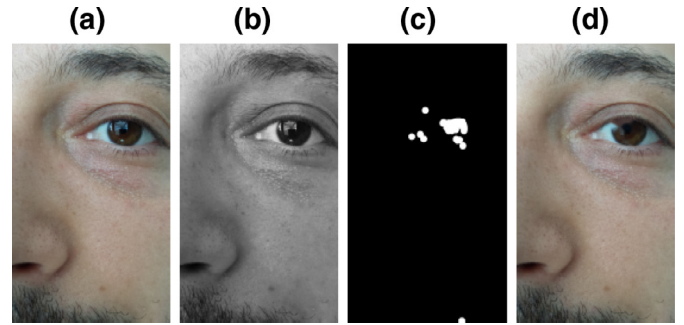


Fig. 2. Iris detected reflections (rightward—source image, blue channel, detected reflections, and their corrections).

Anyhow, contrary to our method none of these NICE methods use true multispectral information. The source images (which are in RGB color space) are typically either converted to gray-scale before any analytical steps or only one spectrum channel is used. The 2008 NICE.I best method by Tan et al. [35] uses clustering for iris localization followed with prediction and curvature models for eyelid and eyelash detection. The second best method by Sankowski et al. [31] consists of three steps—threshold based reflections detection, iris boundaries detection based on modified integro-differential operator, and eyelids detection based on parametric modelling. Several other NICE.I algorithms—expert system [9], K-means clustering in the co-occurrence histogram [16] or methods using NICE.I data and methodology—Markovian texture model [13], and Zernike feature based classification [34], are used to compare the presented method.

The multilayered perceptron neural network based method [23] uses local mean and standard deviation features computed in hue, blue, and red chroma color components. Unlike our presented method, it does not use true textural representation, neglects information due to spectral correlation, and contains several ad hoc selected parameters.

The presented paper extends the method [13] with modified Daugman operator, polynomial upper eyelid model, blue spectral channel reflection detection, separate lower eyelid detection, and it is applied for unconstrained high resolution iris images. These changes simultaneously improved method's performance on the NICE.I contest setup from third position of our previous method [13] to the presented method leading position.

2. Reflection correction

The iris defect detection starts with searching for reflections (Figs. 2(a) and 3(c)) in the blue spectral channel where they are most visible using an adaptive threshold. The binarization threshold is obtained using the cross-correlation between pixel-centered windows and the Gaussian window. The resulting binary mask is firstly slightly dilated (Fig. 2(c)) to ensure full coverage of reflections and then the detected reflective regions are corrected (Fig. 2(d)) using the inpainting algorithm presented in [36].

The corrected multispectral image is subsequently used to detect iris location in the image.

3. Iris localization

The iris defect detection requires to localize the eye region in the acquired image which is complicated with variable source image resolution. The accurate eye region is recognized using a two step procedure with rough localization using the generalized Hough transformation (GHT) subsequently elaborated by a modified integro-differential Daugman operator.

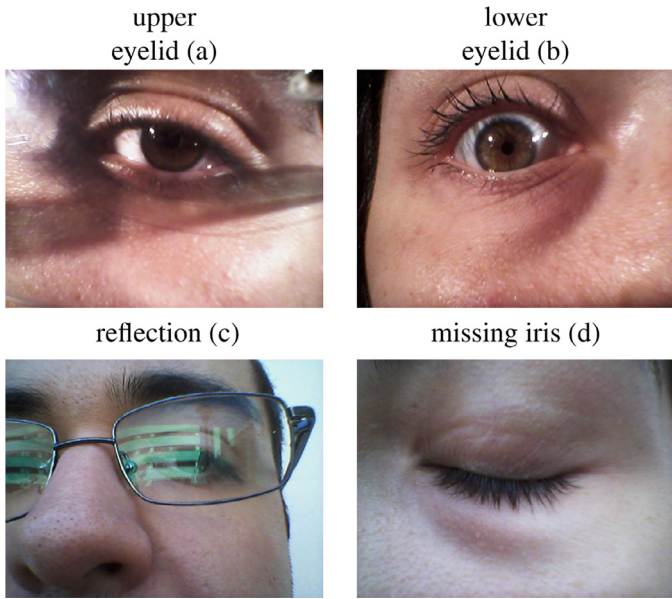


Fig. 3. Iris region defects from iPhone5 device containing all four (a,b,c,d) occlusion types.

3.1. Rough iris localization

The generalized Hough transformation [2] is used to detect approximate eye region on a sub-sampled reflection corrected image. The rough scale image has the width in the range 200–400 pixels because the corresponding sub-sampling step is selected to avoid non-lattice pixel positions interpolation. Down-scaled images speed up the processing time. A binary eye template for GHT is created as the intersection of two circles which are parameterized by the length c of their common chord. It is subsequently rescaled to handle variable image resolution. We assume the ratios of both circular segments altitudes h_1, h_2 to this chord to be fixed

$$k_1 = \frac{c}{h_1} = 4.8,$$

$$k_2 = \frac{c}{h_2} = 15.8.$$

The corresponding circles radii can be computed from

$$R_i = \frac{c^2}{8h_i} + \frac{h_i}{2} = c \frac{k_i^2 + 4}{8k_i} \quad i = 1, 2. \quad (1)$$

This template (Fig. 5 (second image)) is rotated in the range of $\pm 15^\circ$.

3.2. Refined iris localization

The accurate eye area is found using the integro-differential Daugman operator [8] generalized from monospectral into the multispectral formulation (2) to exploit all available information. The multispectral Daugman operator is

$$\max_{\rho, \bar{r}_1, \bar{r}_2} \left| G_\sigma(\rho) \otimes \frac{\partial}{\partial \rho} \oint_{\rho, \bar{r}_1, \bar{r}_2} \frac{Y_{r,\bullet}}{2\pi\rho} ds d\rho \right|, \quad (2)$$

where $r = \{r_1, r_2\}$, $s = \{s_1, s_2\}$ are multiindices with the row and column indices, \bullet denotes all corresponding spectral indices, \bar{r} the radius center, ρ is the radius, $Y_{r,\bullet}$ is the r th multispectral (color) eye pixel, \otimes denotes multispectral convolution, and $G_\sigma(\rho)$ denotes a 3D Gaussian filter of identical scale σ in all spectral planes. The circle integral is not taken for full circle but only for degrees from 0° to 45° and from 135° to 360° . This is to better deal with possible upper eyelid occlusions in image (which would otherwise obviously obstructed the correct localization of iris region). The next step is the pupil border detection

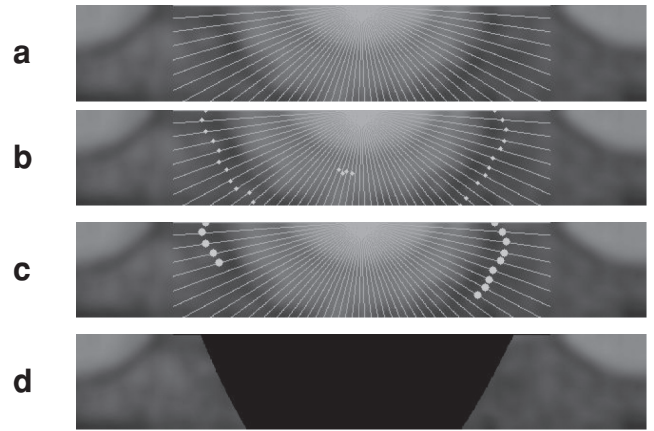


Fig. 4. Upper eyelid detection steps in the red spectral channel.

in the red spectral channel to separate iris region. The inner circle representing pupil border is found (see Fig. 6, odd columns images) in a similar way as the iris location described above but in its respective smaller area. The pupil is detected using the original (unmodified) Daugman operator [8] inside the iris region. Detected iris region is then verified by checking the candidate pupil region mean with comparison of the closest left and right neighborhood iris regions. This is to deal with possible mislocalization of iris border.

4. Iris occlusions and reflection detection

Once we locate the iris region, this region is then normalized to rectangular shape [8] and we subsequently search (see Fig. 1 scheme) for each of the selected defects as it is illustrated in Fig. 3. The rare cases of completely missing irises (Fig. 3(d)) are solved using a simple thresholding in the generalized Hough transformation space. Possible occlusions are searched in the red spectral channel and reflections in the blue spectral channel, respectively.

4.1. Upper eyelid

The upper eyelid (Fig. 3(a)) is detected using vertically swapped image so that a potential upper eyelid is completely located in the center of image (otherwise it would be split in half at the corners of normalized iris image). Subsequently the rays from 0° to 180° from the top center point are drawn (Fig. 4(a)). These rays are convolved with differential kernel and the maximum is located on each of them (Fig. 4(b)) and lower maxima values are removed as potential outliers (Fig. 4(c)). The third order fitted polynomial then denotes the upper eyelid occlusion region border (Fig. 4(d)).

4.2. Lower eyelid

Most iris images are not obstructed with the lower eyelid. The occasional lower eyelid occlusions (Fig. 3 (middle)) are detected using mean and standard deviation estimates μ_{le} and σ_{le} of the top center region. Rows are in the range of $r_1 \in \langle 0; \frac{N}{2} \rangle$ and columns $r_2 \in \langle \frac{M}{4}; \frac{3M}{4} \rangle$, where N (M) is number of rows (columns) in the normalized iris image. If the standard deviation is larger than 25% of μ_{le} , i.e., $\sigma_{le} > \frac{\mu_{le}}{4}$ then the lower eyelid is detected by simple thresholding with the threshold $\tau = \mu + \frac{\sigma_{le}}{2}$. The topmost central region is detected as the lower eyelid in the resulting binarized image.

4.3. Iris reflections

The precise localization of reflections (Fig. 3(right)) in the fine scale normalized iris is based on fusion of similar (without dilatation)

adaptive thresholding as in Section 2 and detection based on the multispectral Markovian iris texture model.

4.3.1. Iris spectral texture model

We assume that the multispectral iris texture can be represented by an adaptive 3D causal simultaneous auto-regressive model [12]:

$$X_r = \sum_{s \in I_r^c} A_s X_{r-s} + \epsilon_r, \quad (3)$$

where ϵ_r is a white Gaussian noise vector with zero mean, and a constant but unknown covariance matrix Σ . The noise vector is uncorrelated with data from a causal neighborhood I_r^c , and $r = \{r_1, r_2\}$, $s = \{s_1, s_2\}$ are multiindices with the row and column indices, respectively.

$$A_{s_1, s_2} = \begin{pmatrix} a_{1,1}^{s_1, s_2}, \dots, a_{1,d}^{s_1, s_2} \\ \vdots \\ a_{d,1}^{s_1, s_2}, \dots, a_{d,d}^{s_1, s_2} \end{pmatrix} \quad (4)$$

are $d \times d$ parameter matrices where d is the number of spectral bands. $r, r-1, \dots$ is a chosen direction of movement on the image lattice (e.g. scanning lines rightward and top to down).

All parameters in this model can be analytically estimated using numerically robust recursive statistics hence it is exceptionally well suited for possibly real-time recursive iris texture defect detectors. The model adaptivity is introduced using the exponential forgetting factor technique in the parameter learning part of the algorithm. The model can be alternatively written in the matrix form

$$X_r = \gamma Z_r + \epsilon_r, \quad (5)$$

where $\gamma = [A_1, \dots, A_\eta]$, $\eta = \text{card}(I_r^c)$ is a $d \times d\eta$ parameter matrix and Z_r is a corresponding vector of X_{r-s} . To evaluate the conditional mean values $E\{X_r | X^{(r-1)}\}$, where $X^{(r-1)}$ is the past process history, the one-step-ahead prediction posterior density $p(X_r | X^{(r-1)})$ is needed. If we assume the normal-gamma parameter prior for parameters in (3) this posterior density has the form of Student's probability density with $\beta(r) - d\eta + 2$ degrees of freedom. The predictor in the form of conditional mean value (10) uses the following notation (6)–(9):

$$\beta(r) = \beta(0) + r - 1, \quad (6)$$

$$\hat{\gamma}_{r-1}^T = V_{zz(r-1)}^{-1} V_{zx(r-1)}, \quad (7)$$

$$V_{r-1} = \begin{pmatrix} \tilde{V}_{xx(r-1)} & \tilde{V}_{zx(r-1)}^T \\ \tilde{V}_{zx(r-1)} & \tilde{V}_{zz(r-1)} \end{pmatrix} + I, \quad (8)$$

$$\tilde{V}_{uw(r-1)} = \sum_{k=1}^{r-1} U_k W_k^T, \quad (9)$$

where $\beta(0) > 1$ and U, W in (9) denote either X or Z vector, respectively. If $\beta(r-1) > \eta$ then the conditional mean value is

$$E\{X_r | X^{(r-1)}\} = \hat{\gamma}_{r-1} Z_r \quad (10)$$

and it can be efficiently computed using the following recursion

$$\hat{\gamma}_r^T = \hat{\gamma}_{r-1}^T + \frac{V_{z(r-1)}^{-1} Z_r (X_r - \hat{\gamma}_{r-1} Z_r)^T}{1 + Z_r^T V_{z(r-1)}^{-1} Z_r}. \quad (11)$$

The selection of an appropriate model support (I_r^c) is important to obtain good iris representation. If the contextual neighborhood is too small it cannot capture all details of the random field iris texture model. Inclusion of the unnecessary neighbors on the other hand adds to the computational burden and can potentially degrade the performance of the model as an additional source of noise. The optimal Bayesian decision rule for minimizing the average probability of decision error chooses the maximum posterior probability model, i.e., a model M_j corresponding to $\max_j \{p(M_j | X^{(r-1)})\}$ can be easily found analytically [12].

4.3.2. Defect detection

Single multispectral pixels are classified as belonging to the defective (non-iris) area based on their corresponding prediction errors. If the prediction error is larger than the adaptive threshold:

$$|\tilde{E}\{X_r | X^{(r-1)}\} - X_r| > \frac{\alpha}{l} \sum_{i=1}^l |\tilde{E}\{X_{r-i} | X^{(r-i-1)}\} - X_{r-i}|, \quad (12)$$

then the pixel r is classified as a detected defect pixel. The parameter l in (13) is a process history length of the adaptive threshold and the constant $\alpha = 2.7$ was found experimentally.

The one-step-ahead predictor

$$\tilde{E}\{X_r | X^{(r-1)}\} = \hat{\gamma}_s Z_r \quad (13)$$

differs from the corresponding predictor (10) in using parameters $\hat{\gamma}_s$ which were learned only in the flawless texture area ($s < r$). The small learning flawless texture cutout is found automatically inside reflection-less iris area. The whole algorithm is extremely fast because the adaptive threshold is updated recursively:

$$|\epsilon_{r+1}| > \frac{\alpha}{l} \left[\sum_{i=0}^{l-1} |\epsilon_{r-i}| \right], \quad (14)$$

where ϵ_r is the prediction error

$$\epsilon_r = \tilde{E}\{X_r | X^{(r-1)}\} - X_r, \quad (15)$$

and $\hat{\gamma}_s$ is the parametric matrix which is not changing. Hence the algorithm can be easily applied in real time iris defect detection.

5. Experimental results

The presented method was tested on the MICHE [21] and UBIRIS v2 [25] databases.

The MICHE images were captured by three mobile devices iPhone5 (1262 images), Samsung Galaxy S4 (1297 images), and Samsung Galaxy Tab2 (632 images). First two devices exploited both available cameras, i.e. 8 mega-pixel (MPx) iSight camera and 1.2 MPx FaceTime camera in iPhone5 and Samsung Galaxy S4 13 and 2 Mpx cameras, while only the front VGA camera was used in Samsung Galaxy Tab2. For all 72 subjects were taken between 4 and 8 images per person in an unconstrained outdoor and indoor environments. Some MICHE details are listed in Table 1. Each person has recorded the same eye (left or right) using both (rear-facing as well as front-facing) cameras with the 72 dpi resolution together with information about age and gender. Selected results from the iPhone5 both cameras are illustrated in Fig. 6. Similar results were achieved on the remaining mobile devices as illustrated on the partial results from Samsung Galaxy S4 (Fig. 5). There are not available ground truth data for the MICHE database thus these results can be verified only visually, thus we included also our method comparison with the results from the Noisy Iris Challenge Evaluation Contest, where such numerical results are accessible. The alternative NICE.I methods have no public code thus we cannot use them for visual comparison on the MICHE database.

Table 1
MICHE iris database.

	(Number of images) Resolution	Distance [cm]
iPhone5	(1262)	
Front camera	960 × 960, 960 × 1280	≈ 10
Rear camera	1536 × 2048, 2448 × 2448	
	2448 × 3264	≈ 13
Samsung Galaxy S4	(1297)	
Front camera	1080 × 1920	≈ 10
Rear camera	2320 × 4128	≈ 13
Samsung Galaxy Tab2	(632)	
Front camera	640 × 480	≈ 5

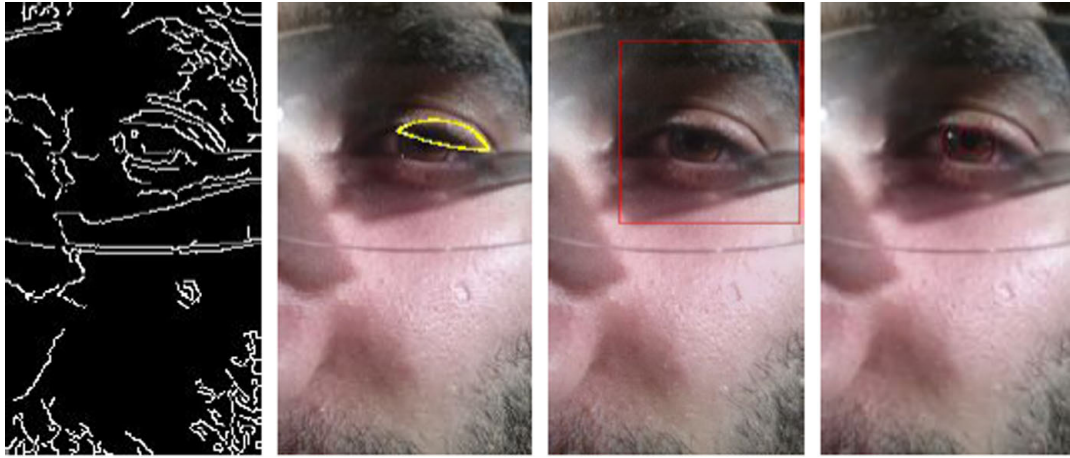


Fig. 5. Detected rough iris region using the generalized Hough transformation (rightward Canny detector, GHT mask, search window, detected iris).

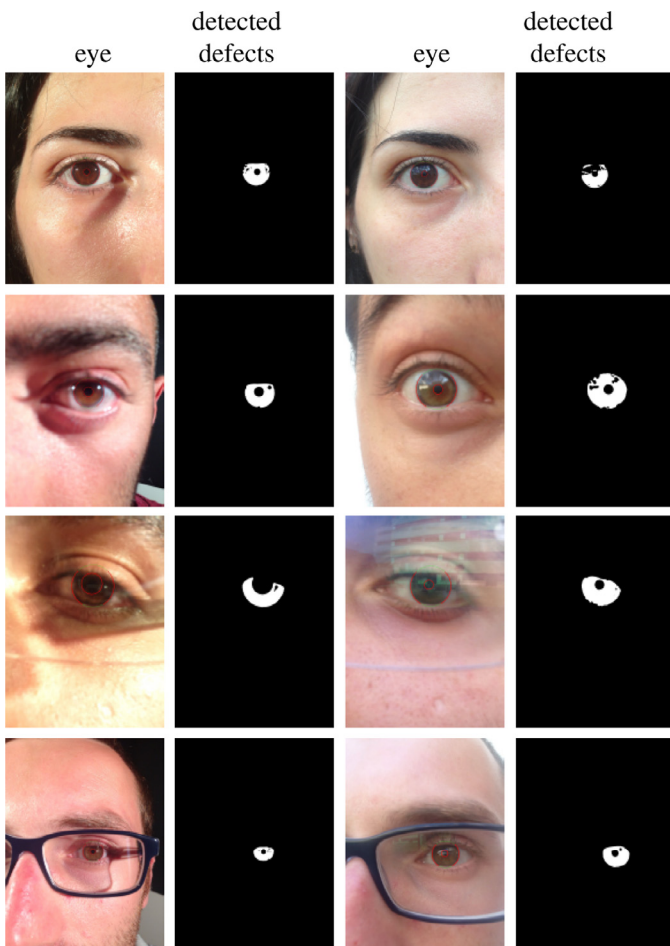


Fig. 6. Selected eye images from the MICHE database and their detected defects.

The presented method was evaluated on the eye UBIRIS v2 database [25] and compared with the best results achieved during the Noisy Iris Challenge Evaluation contest [28]. Although the UBIRIS v2 data are different and less challenging than the MICHE data, there is ground truth available and nearly hundred alternative results from the NICE contest which can be used for comparison and result ranking. These databases provide eye images with or without different occlusion types (Fig. 3), and thus are an useful resource for the evaluation iris recognition methods. The UBIRIS.v2 database [29] contains

Table 2

Iris defect detection Noisy Iris Challenge Evaluation Contest [28] top eight results comparison.

Rank	Method	Number of parameters	Error
1	Presented method	7	0.0124
2	Tan et al. [35]	9	0.0131
3	Sankowski et al. [31]	6	0.0162
4	Haindl and Krupička [13]	2	0.0168
5	Almeida [9]	5	0.0180
6	Tan and Kumar [34]	Unknown	0.0190
7	Li et al. [19]	4	0.0224
8	Jeong et al. [16]	3	0.0282
9	Chen et al. [5]	5	0.0297
10	Scotti and Labbati [18]	12	0.0301
11	Luengo-Oroz et al. [20]	7	0.0305

11,102 images collected from 261 persons. The RGB 400×300 , 24 bit images were captured with the Canon EOS 5D camera and saved in the TIFF format. The presented method was compared with the top eight results (from 97 participants) [5,9,16,18–20,31,35] from the Noisy Iris Challenge Evaluation Contest (NICE.I) [28] and results using the same NICE.I data presented in the paper [34]. All comparisons (Table 2) obey the NICE.I contest protocol [27]. The contest was run on the UBIRIS.v2 database which contains highly noisy eye images. The participants had 500 training images and a disjoint test set of 500 images was used to measure the pixel-by-pixel agreement between the binary maps made by each participant (X) and the ground-truth data (G), manually built by the NICE.I organizers [27]:

$$\text{Error} = \frac{1}{mn_r n_c} \sum_{k=1}^n \sum_{r_1=1}^{n_r} \sum_{r_2=1}^{n_c} n X_r \otimes n G_r, \quad (16)$$

where \otimes is the logic XOR operator, n_r , n_c , n are the number of rows, columns, and testing images, respectively.

Fig. 7 indicates several types of defective iris textures. This example illustrates correct detection and localization of the most frequent iris occlusion by the presented method.

The presented method ranked first (Table 2) according to the contest criterion Error (16) on the contest test set. The Noisy Iris Challenge Evaluation Contest winning algorithm [35] has slightly worse performance than the presented method but it is very complex, time consuming and suffers with numerous experimentally set control parameters. Similarly the third ranked method [31] based on the reflections localization, reflections filling in, iris boundaries localization and eyelids boundaries localization steps, relies on several experimentally found parameters.

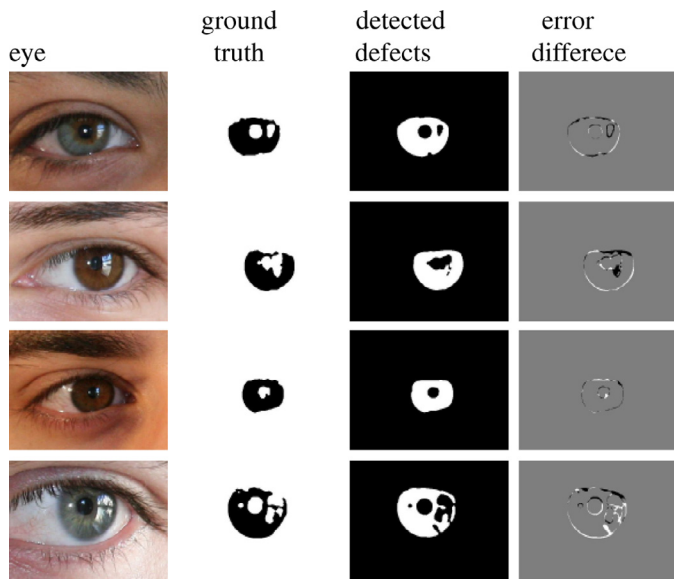


Fig. 7. Eye images from the UBIRIS v2 database, ground truth, detected occlusions masks, and their comparison with the ground truth.

6. Conclusions

The most published iris defect detection methods are monospectral using near-infrared measurements, while our method advantageously exploits both multispectral as well as the spatial information simultaneously. The method uses the multispectral generalization of the Daugman operator, polynomial upper eyelid model, and fully multispectral spatial Markovian texture model. The method is very fast and robust in comparison with the top-ranking alternative methods from the NICE.I contest. Our method ranked first when evaluated on the Noisy Iris Challenge Evaluation Contest from the 97 competing algorithms and the Tan method.

Visual results demonstrate its promising performance also on the very challenging and highly variable Mobile Iris Challenge Evaluation data. The presented method can be easily generalized for gradually changing (e.g., illumination, color, etc.) iris texture defect detection by exploiting its adaptive learning capabilities.

Acknowledgment

This research was supported by the Czech Science Foundation project GAČR 14-10911S.

References

- [1] F.H. Adler, *Physiology of the Eye: Clinical Application*, The C.V. Mosby Co., St. Louis, 1959.
- [2] D.H. Ballard, Generalizing the hough transform to detect arbitrary shapes, *Pattern Recogn.* 13 (2) (1981) 111–122.
- [3] K.W. Bowyer, K. Hollingsworth, P.J. Flynn, Image understanding for iris biometrics: A survey, *Comput. Vis. Image Underst.* 110 (2) (2008) 281–307.
- [4] M.J. Burge, K.W. Bowyer, *Handbook of Iris Recognition*, Springer, 2013.
- [5] Y. Chen, M. Adjouadi, C. Han, J. Wang, A. Barreto, N. Rische, J. Andrian, A highly accurate and computationally efficient approach for unconstrained iris segmentation, *Image Vis. Comput.* 28 (2) (2010) 261–269.
- [6] Y. Chen, S.C. Dass, A.K. Jain, Localized iris image quality using 2-d wavelets, *Adv. Biomet.* (2005) 373–381.

- [7] D. Chetverikov, Detecting defects in texture, in: *International Conference on Pattern Recognition*, 1988, pp. 61–63.
- [8] J. Daugman, High confidence visual recognition of persons by a test of statistical independence, *IEEE Trans. Pattern Anal. Mach. Intell.* 15 (11) (1993) 1148–1161.
- [9] P. de Almeida, A knowledge-based approach to the iris segmentation problem, *Image Vis. Comput.* 28 (2) (2010) 238–245.
- [10] Y. Du, R. Ives, D. Etter, A new approach to iris pattern recognition, *Proc. SPIE* (2004) 1–12.
- [11] H. Fujiwara, Z. Zhang, H. Toda, H. Kawabata, Textile surface inspection by using translation invariant wavelet transform, in: *IEEE International Symposium on Computational Intelligence in Robotics and Automation*, 3, IEEE, 2003, pp. 1427–1432.
- [12] M. Haindl, L. Florack, R. Duits, G. Jongbloed, M.C. Lieshout, L. Davies, *Mathematical Methods for Signal and Image Analysis and Representation*, Springer, London, 2012, pp. 241–259.
- [13] M. Haindl, M. Krupička, Non-iris occlusions detection, in: *2013 IEEE Sixth International Conference on Biometrics: Theory, Applications and Systems (BTAS)*, IEEE, 2013, pp. 1–6.
- [14] R. Haralick, K. Shanmugam, I. Dinstein, Textural features for image classification, *IEEE Trans. Syst. Man Cybernet.* 3 (6) (1973) 610–621.
- [15] Z. He, T. Tan, Z. Sun, X. Qiu, Toward accurate and fast iris segmentation for iris biometrics, *IEEE Trans. Pattern Anal. Mach. Intell.* 31 (9) (2009) 1670–1684.
- [16] D.S. Jeong, J.W. Hwang, B.J. Kang, K.R. Park, C.S. Won, D.K. Park, J. Kim, A new iris segmentation method for non-ideal iris images, *Image Vis. Comput.* 28 (2) (2010) 254–260.
- [17] A. Kumar, Inspection of surface defects using optimal fir filters, in: *ICASSP*, vol. II, IEEE, 2003, pp. 241–244.
- [18] R.D. Labati, F. Scotti, Noisy iris segmentation with boundary regularization and reflections removal, *Image Vis. Comput.* 28 (2) (2010) 270–277.
- [19] P. Li, X. Liu, L. Xiao, Q. Song, Robust and accurate iris segmentation in very noisy iris images, *Image Vis. Comput.* 28 (2) (2010) 246–253.
- [20] M.A. Luengo-Oroz, E. Faure, J. Angulo, Robust iris segmentation on uncalibrated noisy images using mathematical morphology, *Image Vis. Comput.* 28 (2) (2010) 278–284.
- [21] M.D. Marsico, C. Galdi, M. Nappi, D. Riccio, Firme: Face and iris recognition for mobile engagement, *Image Vis. Comput.* 32 (2014) 1161–1172.
- [22] R. Meylani, A. Ertuzun, A. Eril, A comparative study on the adaptive lattice filter structures in the context of texture defect detection, in: *ICECS'96*, vol. II, 1996, pp. 976–979.
- [23] H. Proença, Iris recognition: On the segmentation of degraded images acquired in the visible wavelength, *IEEE Trans. Pattern Anal. Mach. Intell.* 32 (8) (2010) 1502–1516.
- [24] H. Proença, L. Alexandre, Iris recognition: Measuring feature's quality for the feature selection in unconstrained image capture environments, in: *Proceedings of the 2006 IEEE International Conference on Computational Intelligence for Homeland Security and Personal Safety*, IEEE, 2006, pp. 35–40.
- [25] H. Proença, L.A. Alexandre, UBIRIS: A noisy iris image database, in: *13th International Conference on Image Analysis and Processing (ICIAP'05)*, Springer, Cagliari, Italy, 2005, pp. 970–977.
- [26] H. Proença, L.A. Alexandre, A method for the identification of noisy regions in normalized iris images, in: *18th International Conference on Pattern Recognition (ICPR'06)*, vol. 4, 2006, pp. 405–408.
- [27] H. Proença, L.A. Alexandre, The nice.II: Noisy iris challenge evaluation—Part I, in: *First IEEE International Conference on Biometrics: Theory, Applications, and Systems (BTAS'07)*, IEEE, 2007, pp. 1–4.
- [28] H. Proença, L.A. Alexandre, Introduction to the special issue on the segmentation of visible wavelength iris images captured at-a-distance and on-the-move, *Image Vis. Comput.* 28 (2) (2010) 213–214.
- [29] H. Proença, S. Filipe, R. Santos, J. Oliveira, L. Alexandre, The ubiris.v2: A database of visible wavelength iris images captured on-the-move and at-a-distance, *IEEE Trans. Pattern Anal. Mach. Intell.* 32 (8) (2010) 1529–1535.
- [30] C. Rathgeb, A. Uhl, P. Wild, *Iris Biometrics: From Segmentation to Template Security*, vol. 59, Springer, 2013.
- [31] W. Sankowski, K. Grabowski, M. Napieralska, M. Zubert, A. Napieralski, Reliable algorithm for iris segmentation in eye image, *Image Vis. Comput.* 28 (2) (2010) 231–237.
- [32] W. Sankowski, K. Grabowski, M. Zubert, M. Napieralska, Iris finder—program for reliable iris localization in images taken under visible light vol. 10 (2006) 125–132.
- [33] J.L. Sobral, Optimised filters for texture defect detection, in: *International Conference on Image Processing*, vol. III, 2005, pp. 565–568.
- [34] C.W. Tan, A. Kumar, Unified framework for automated iris segmentation using distantly acquired face images, *IEEE Trans. Image Process.* 21 (9) (2012) 4068–4079.
- [35] T. Tan, Z. He, Z. Sun, Efficient and robust segmentation of noisy iris images for non-cooperative iris recognition, *Image Vis. Comput.* 28 (2) (2010) 223–230.
- [36] A. Telea, *J. Graphic Tool* 9 (1) (2004) 23–34.
- [37] R.P. Wildes, Iris recognition: An emerging biometric technology, *Proc. IEEE* 85 (9) (1997) 1348–1363.